Field-Tuned Order by Disorder in Frustrated Ising Magnets with Antiferromagnetic Interactions

P. C. Guruciaga,[1] M. Tarzia,[2] M. V. Ferreyra,[3] L. F. Cugliandolo,[4] S. A. Grigera,[3,5] and R. A. Borzi[3,*]
[1]*Instituto de Investigaciones Físicas de Mar del Plata (IFIMAR), UNMdP-CONICET, 7600 Mar del Plata, Argentina*
[2]*Université Pierre et Marie Curie—Paris 6, Laboratoire de Physique Théorique de la Matière Condensée, 4, Place Jussieu, Tour 13, 5ème étage, 75252 Paris Cedex 05, France*
[3]*Instituto de Física de Líquidos y Sistemas Biológicos (IFLYSIB), UNLP-CONICET, 1900 La Plata, Argentina*
[4]*Université Pierre et Marie Curie—Paris 6, Laboratoire de Physique Théorique et Hautes Energies, 4, Place Jussieu, Tour 13, 5ème étage, 75252 Paris Cedex 05, France*
[5]*School of Physics and Astronomy, University of St Andrews, St Andrews KY16 9SS, United Kingdom*
(Received 9 June 2016; published 14 October 2016)

We demonstrate the appearance of thermal order by disorder in Ising pyrochlores with staggered antiferromagnetic order frustrated by an applied magnetic field. We use a mean-field cluster variational method, a low-temperature expansion, and Monte Carlo simulations to characterize the order-by-disorder transition. By direct evaluation of the density of states, we quantitatively show how a symmetry-broken state is selected by thermal excitations. We discuss the relevance of our results to experiments in 2D and 3D samples and evaluate how anomalous finite-size effects could be exploited to detect this phenomenon experimentally in two-dimensional artificial systems, or in antiferromagnetic all-in–all-out pyrochlores like $Nd_2Hf_2O_7$ or $Nd_2Zr_2O_7$, for the first time.

DOI: 10.1103/PhysRevLett.117.167203

Order by disorder (OBD) is the mechanism whereby a system with a nontrivially degenerate ground state develops long-range order by the effect of classical or quantum fluctuations [1]. From a theoretical point of view, the OBD mechanism is a relatively common occurrence in geometrically frustrated spin models [2], such as the fully frustrated domino model—where it was discussed for the first time [1]—or the Ising antiferromagnet on the three-dimensional fcc lattice [3]. Many other theoretical realizations exist. However, definitive experimental evidence for this mechanism has remained elusive. Strong evidence for *quantum* OBD in the antiferromagnetic (AFM) *XY* insulating rare-earth pyrochlore oxide $Er_2Ti_2O_7$ has been reported [4–7], but a conclusive proof of *thermal* OBD remains unseen in the laboratory so far. The difficulty lies in establishing whether order is selected through the OBD mechanism (a huge disproportion in the density of low-energy excitations associated with particular ground states) or is due to energetic contributions not taken into account that actually lift the ground-state degeneracy.

In this work we study OBD in Ising spin systems where the staggered order is inhibited by a magnetic field. We analyze theoretically and numerically the three-dimensional pyrochlore system and its two-dimensional projection (the checkerboard lattice). We demonstrate the existence of singular finite-size effects (FSE) and we show how they can be exploited to detect OBD. Our results suggest that thermal OBD could be finally observed experimentally in natural staggered structures based on the pyrochlores [8–10], as well as in artificially designed two-dimensional magnetic [11] or colloidal systems [12].

More precisely, we first study an Ising pyrochlore with $\langle 111 \rangle$ anisotropy and AFM nearest-neighbor interactions. In the absence of magnetic field ($\mathbf{B}$), the ground state is the all-spins-in–all-spins-out Néel state [13]. A strong field along the crystalline direction [110] can break this order, turning it into a disordered state with three-spins-in–one-spin-out and three-out–one-in elementary units. This type of disordered system of *magnetic charges* (see below) had been studied before in the context of spin ice [14–16], but in the presence of rather artificial constraints. In contrast, as we will show, the present case is obtained in a simple way, with the additional reward of exhibiting an OBD transition at moderate fields. We give numerical evidence for this phenomenon and we prove it analytically with the cluster variational method (CVM) [17] and a low-temperature analysis [1] of the 2D approximate projection on the checkerboard lattice that allow us to exhibit singular FSE [18]. We explicitly show the relevance of the low-energy excitations on the ordering mechanism by evaluating the density of states of the 3D system. Finally, we discuss the possibility to discriminate true OBD experimentally in three different scenarios.

The pyrochlore lattice consists of corner-sharing tetrahedra; see Fig. 1(a). The centers of tetrahedra pointing up (colored) and down (uncolored) make two interpenetrating fcc lattices (a diamond lattice). Classical Ising magnetic moments $\boldsymbol{\mu}_i = \mu \mathbf{S}_i = \mu S_i \hat{\mathbf{s}}_i$ sit on the vertices of the tetrahedra. The quantization directions $\hat{\mathbf{s}}_i$ are along the $\langle 111 \rangle$ diagonals and, conventionally, $S_i = \pm 1$ indicates a magnetic moment pointing outwards or inwards of an up tetrahedron. The Hamiltonian is

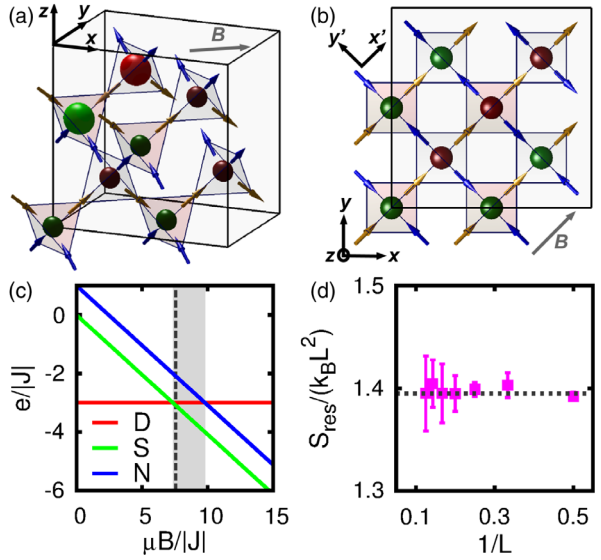

FIG. 1. (a) Conventional unit cell of the pyrochlore lattice ($L = 1$) with 4 tetahedra pointing up (colored) and 4 pointing down (uncolored). The arrows represent the spin direction at each site. The color of the spheres marks the sign of the charges and the size is proportional to their modulus. (b) Planar projected configuration: a tetrahedron becomes a square with crossings, in a checkerboard lattice. The field $\mathbf{B}\|[110]$ couples to two spins on each tetrahedron (α chains, yellow arrows), and is orthogonal to the other two (β chains, blue arrows). The configuration shown is a zero-temperature ground state for large fields. (c) The energy of a singly charged (S), doubly charged (D), and neutral tetrahedron (N) as functions of the magnetic energy normalized by the exchange energy scale; only the energies corresponding to the S and N configurations favored by the field are shown. (d) Linear size dependence of the residual entropy S_{res}.

$$\mathcal{H} = -J_{nn}\sum_{\langle ij\rangle}\mathbf{S}_i\cdot\mathbf{S}_j - \mu\sum_i \mathbf{B}\cdot\mathbf{S}_i, \tag{1}$$

where J_{nn} is the exchange constant, and the first sum runs over nearest neighbors. The ferromagnetic (FM) version of this Hamiltonian corresponds to the nearest-neighbor spin-ice model. Differently from other works, here we concentrate on the antiferromagnetic case. For $\mathbf{B}\|[110]$, one can understand the spin system as consisting of two types of chains: while blue arrows (β spins) belong to the "β chains" (running perpendicular to $\mathbf{B}$) with $\hat{\mathbf{s}}_i\cdot\mathbf{B} = 0$, yellow ones ($\alpha$ spins) sit on the "α chains" (parallel to $\mathbf{B}$), such that $\hat{\mathbf{s}}_i\cdot\mathbf{B} = \alpha_i\sqrt{2/3}B$ and $\alpha_i = \pm 1$ [19]. Figure 1(b) displays the conventional planar projection of the 3D lattice. Using these definitions, one can rewrite the Hamiltonian in terms of scalar quantities:

$$\mathcal{H} = J\sum_{\langle ij\rangle}S_iS_j - \frac{\sqrt{2}\mu B}{\sqrt{3}}\sum_{i\in\alpha}\alpha_iS_i, \tag{2}$$

where $J < 0$ contains a geometrical factor (including a sign change) [20] and the second sum runs over the α chains only.

Within the magnetic charge picture [21], the centers of up or down tetrahedra are considered neutral if two of their spins point in and two out, have a positive or negative single charge if three spins point in and one out, or vice versa [pictured as small spheres in Figs. 1(a) and 1(b)], or a positive or negative double charge if all spins point in or all point out [pictured as big spheres in Fig. 1(a)]. In this language, the ground state for $\mathbf{B} = 0$ consists of an array of double charges of alternating sign with the zinc blende structure, which spontaneously breaks the symmetry between the two fcc sublattices [22]. Unlike the single charges and the neutral state, a double charge has no magnetic moment, making it unstable under a sufficiently strong magnetic field applied along any direction. $\mathbf{B}\|[110]$ is special in that it does so without favoring any fcc sublattice [23], opening the door to a single-charge disordered ground state. In order to measure the amount of charge order for a given spin configuration, we define the single and double staggered charge densities, ρ_S^s and ρ_S^d, respectively. They represent the modulus of the magnetic charge density due to single or double monopoles in up tetrahedra, normalized so that full order corresponds to a value of 1. It is also useful to define $\rho_S = \rho_S^s + 2\rho_S^d$ representing the *total* staggered charge per sublattice site.

As implied by Eq. (2), $\mathbf{B}$ lowers the energy of single charges and neutral tetrahedra with positive projection of magnetic moment along it, leaving that of double charges unchanged [see Fig. 1(c)]. A field B such that $\mu B/|J| > 7.348$ stabilizes a ground state which, while remaining globally neutral, has a single charge on each tetrahedron. This field orders the α chains ferromagnetically [Fig. 1(b)], isolating the β chains in the same way that a [111] field decouples the kagome planes in the spin-ice case [24]. Spins on β chains are impervious to this field but not to the exchange interaction. Each β chain will thus independently and spontaneously order antiferromagnetically [see Fig. 1(b)], implying a spontaneous one-dimensional staggered charge order along each β chain. The additional freedom associated with the symmetry breaking within each separate β chain means that no 3D staggered charge order can arise at $T = 0$, though the residual entropy (proportional to the number of chains, not spins) is subextensive. We tested this fact using Monte Carlo (MC) simulations in a system of L^3 cubic cells and periodic boundary conditions with an applied field $\mu B/|J| = 12.1$, well in the disordered regime. By integrating the specific heat over a wide temperature range ($0.1 < k_BT/|J| < 70$), and through direct calculation from the density of states computed with the Wang-Landau (WL) algorithm [25], we obtained the residual entropy $S_{\text{res}} \propto L^2$ for different system sizes [Fig. 1(d)]. Details on the simulations are provided in the Supplemental Material [26].

Here we are interested in the situation in which the ground state consists of this disordered single-charge state while the lowest energy excitations correspond to double charges [see the shaded area in Fig. 1(c); the dashed line

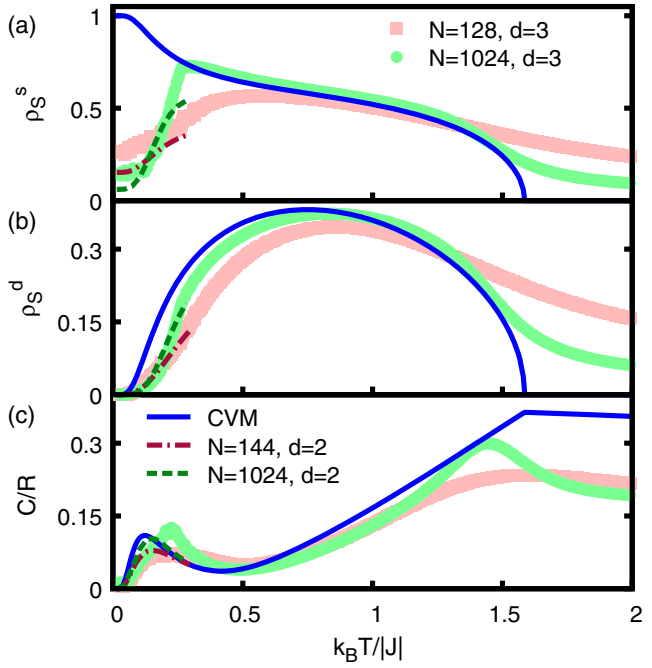

FIG. 2. The order parameters (a) ρ_S^s and (b) ρ_S^d and (c) the specific heat as functions of temperature. The symbols show MC data for the 3D system, and the dashed lines (with the same color code) show the results of the low-T expansion for the 2D projection, both with similar number of spins N. The solid (blue) lines are the CVM outcome ($N \to \infty$).

marks the field $\mu B/|J| = 7.562$ used in the remainder of this work]. The appearance of excitations implies an obvious entropy increase. On the other hand, their structure (all spins in or all out) imposes nearest-neighbor correlations [22] that will favor charge order between adjoining chains, and thus the phenomenon of OBD that we will study.

The CVM places the tetrahedra on a tree with the same coordination number as the 3D lattice, i.e., four [17,28,29] (Husimi tree). Once this is done, recurrence relations for the order parameters are derived and solved analytically in the infinite-size limit. We tested the formation of charge order in the zinc blende structure by measuring ρ_S^d and ρ_S^s, plotted as continuous lines in Fig. 2. Within the CVM both order parameters are strictly zero at $T = 0$. At an infinitesimal temperature ρ_S^s jumps to one and ρ_S^d increases continuously from zero. The two observables vanish at T_c as in a second-order Ising-type phase transition with mean-field exponents. The specific heat at low T has a standard Schottky anomaly due to two-level system excitations. The second peak indicates the transition to the disordered phase and it is just a cusp since $\alpha = 0$ in mean field. The MC simulations of the 3D model (symbols in Fig. 2) clearly support this interpretation of the specific heat, with a low-temperature Schottky anomaly at low T, and a broad peak with evident FSE at T_c [Fig. 2(c)]. Its evolution with the number of spins N, as well as that of $\rho_S^s(T_c)$ and its fluctuations, are consistent with a second-order transition within the 3D Ising universality class (see Supplemental Material [26]). In order to understand better the behavior of the order parameter, we discuss the important low-T finite-size effects below.

A careful low-T analysis is most easily implemented in the projection to the checkerboard lattice. As in the 3D case, the lowest energy levels are excited by flipping an α spin against $\mathbf{B}$. Furthermore, this α spin should link two β chains with *staggered* AFM 1D order. Labeling the spins s_{ij} in Fig. 1(b) according to the coordinate system $(0; x, y)$, such an excitation would be to turn the spin s_{22}. This creates two defects with an energy cost equal to $2\epsilon = 2\mu B - 12J$ ($\epsilon/J = 0.164$ for the parameters of the numerical simulations). For simplicity, we used open boundary conditions in this representation.

With the exact enumeration of these excitations we calculated ρ_S^s and ρ_S^d for finite N at low T. We expect the FSE to depend on the number of spins N on the lattice, independently of its dimension d. We see in Fig. 2 that the behavior observed for $d = 2$ qualitatively follows that of the numerical simulations of the 3D system. The naive extrapolation of ρ_S^s in the low-T limit for $N \to \infty$ suggests that ρ_S^s vanishes in the thermodynamic limit, in seeming contradiction to the CVM results (top of Fig. 2). To explain this, we provide below a careful study of the interplay between the limits $N \to \infty$ and $\beta\epsilon \to \infty$ in the checkerboard model.

Consider two neighboring β chains with M spins in the direction y' of the rotated coordinate system $(0; x', y')$ in Fig. 1(b) [30]. In the low-T limit the β spins have perfect antiferromagnetic order along the y' direction. There are thus two possibilities for the relative orientation of the spins on neighboring β chains: they are either parallel [FM ordered, e.g., the second and third β chains in Fig. 1(b)] or antiparallel [AFM ordered, e.g., in the first and second β chain in Fig. 1(b)]. In the latter case and for M large enough, there are $O(M/2)$ possible excitations of energy 2ϵ, obtained by reversing an α spin between the two β chains, and the partition function is $Z_{\mathrm{AFM}} \simeq (1 + e^{-2\beta\epsilon})^{M/2}$. In the former case there are no possible low-energy excitations (neglecting the presence of neutral tetrahedra) and $Z_{\mathrm{FM}} \simeq 1$. This can be interpreted in terms of an effective AFM coupling between the β spins only. Let us compare the partition functions for the two possible orientations,

$$\frac{Z_{\mathrm{AFM}}}{Z_{\mathrm{FM}}} = e^{-\beta(H_{\mathrm{eff}}^{\mathrm{AFM}} - H_{\mathrm{eff}}^{\mathrm{FM}})}, \qquad H_{\mathrm{eff}} = J_{\mathrm{eff}} \sum_{j'=1}^{M} s_{1j'}^{\beta} s_{2j'}^{\beta}, \tag{3}$$

where $s_{i'j'}^{\beta}$ label the β spins and i', j' sweep the rotated lattice in Fig. 1(b). The interaction on each β chain remains the original J. Then $H_{\mathrm{eff}}^{\mathrm{AFM}} = -J_{\mathrm{eff}} M$, $H_{\mathrm{eff}}^{\mathrm{FM}} = J_{\mathrm{eff}} M$, and we conclude that J_{eff} is given by

$$J_{\mathrm{eff}} = (4\beta)^{-1} e^{-2\beta\epsilon}. \tag{4}$$

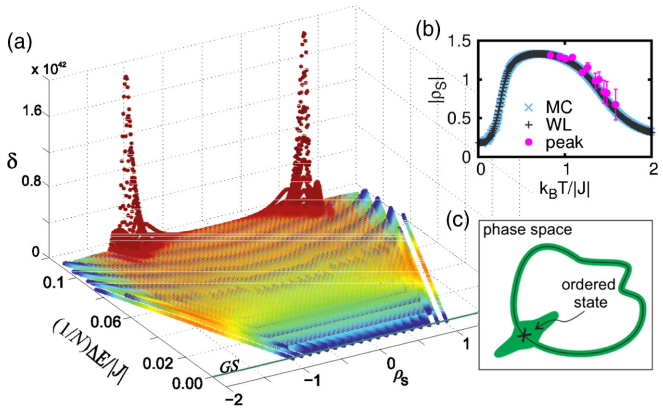

FIG. 3. (a) Density of states δ as a function of excitation energy ΔE and total staggered charge density ρ_S, for a system of size $L = 3$ and for $\mu B/|J| = 7.562$. Each colored circle corresponds to a single energy of the system. The two symmetric peaks are centered at $|\rho_S^{\text{peak}}| \approx 1.2$. Inset (b) compares $|\rho_S|$ calculated from the WL method and the MC simulation with the values directly obtained from the maxima of δ. Inset (c), copied from Ref. [31], represents the ground-state manifold (black curve) in parameter space and the selection of an ordered state (cross) by thermal excitations (green region).

Thus, after integrating out the α spins, we have an effective low-T model on a tilted 2D square lattice, with AFM *anisotropic* interactions equal to J in the y' direction and J_{eff} in the x' direction.

We now go one step further and we reduce the low-T effective model to a 1D one. As mentioned, the β chains are perfectly ordered for $k_B T/|J| \ll 1$. We define a macro β spin $\sigma = +1$ (-1) according to the direction of the first spin on the chain being up (down). They sit on the sites of a 1D lattice and interact with an effective AFM interaction MJ_{eff}. The $T \to 0^+$ limit is then very tricky, since $J_{\text{eff}} \to 0$ in a singular way. At any finite M, $MJ_{\text{eff}} \to 0$ for $T \to 0^+$: the effective 1D system decouples and disorders. However, if we take $M \to \infty$ first, the effective 1D system orders AFM and, as it was already AFM ordered along the β chains, it is fully AFM ordered with $\rho_S^s \xrightarrow[T\to 0^+]{} 1$. In conclusion, the low-T expansion predicts a first-order OBD transition with a finite jump of ρ_S^s from 0 to 1, just as obtained with the CVM. One has

$$0 = \lim_{N\to\infty} \lim_{T\to 0^+} \rho_S^s \neq \lim_{T\to 0^+} \lim_{N\to\infty} \rho_S^s = 1. \tag{5}$$

MC results are not in contradiction with this: huge values of N are needed to see a large ρ_S^s as T lowers [Fig. 2(a)].

OBD is sometimes illustrated by a cartoon [2,31] in which the ground-state manifold is represented by a curve in phase space [see Fig. 3(c)]. The increment on the accessible phase space when raising T slightly from 0 is drawn as a surface (green) next to this curve. OBD occurs when the excitations linked to certain ordered ground states (cross) dominate the thermal average over all accessible states. We can turn this description into a quantitative argument by explicitly calculating the density of states $\delta(\Delta E, \rho_S)$ of the 3D system with the WL algorithm. We move along the configuration space using two parameters: the energy excess with respect to the ground state ΔE and the total staggered charge density ρ_S. Figure 3 shows the low-energy part of δ for $L = 3$ and the same magnetic field used in Fig. 2. The colors emphasize the value of δ, normalized using that there is a single state with $\rho_S = 2$ (a double monopole crystal). Each point in the graph represents the real binning in energy and order parameter. We can see a very flat surface near the degenerate ground-state energy ($\Delta E = 0$) and two very noticeable symmetric peaks; e.g., at $\Delta E/(N|J|) = 0.106$ the maxima are at $\rho_S^{\text{peak}} \approx \pm 1.2$. Consistently, the MC canonical ensemble average of the order parameter and the one computed with

$$|\rho_S|^{\text{WL}} = \frac{1}{\mathcal{Z}} \sum_{\Delta E_k}^{\Delta E_k^{\max}} \sum_{\rho_{Sl}} |\rho_{Sl}| \delta(\Delta E_k, \rho_{Sl}) e^{-\beta \Delta E_k}, \tag{6}$$

with $\Delta E_k^{\max}/|J| = 0.385$, coincide over a rather wide range of T; see Fig. 3(b). The remaining (pink) data points are obtained as follows. We first read the density $\rho_S^{\text{peak}}(\Delta E)$ that maximizes δ for each ΔE. Such an evaluation is quite precise on the interval $\Delta E/(N|J|) \in [0.05, 0.2]$ and it coincides, within numerical accuracy, with $|\rho_S|(\langle \Delta E \rangle)$ measured with the MC or WL methods (not shown). We next transform the ΔE dependence into a T dependence replacing ΔE by $\langle \Delta E \rangle(T)$ from the MC data. We therefore obtain $|\rho_S^{\text{peak}}|(T)$ in Fig. 3(b). The good coincidence between the data points obtained in this way and through Eq. (6) marks the importance of low-energy thermal fluctuations around the ordered states. Furthermore, the procedure complements the low-T expansion in the sense that it estimates $|\rho_S|$ beyond its maximum as a function of T.

We will now discuss how an experimental contrast to our results may be possible with magnetic [8–11,32] or colloidal [12] samples. In order to observe classical OBD experimentally in these systems, the tendency towards a charge ordered ground state favored by a misaligned **B** or long-range dipolar interactions should be made as small as possible. A first option are the AFM Ising pyrochlores [8–10]. They have the advantage that the stabilization of the all-in–all-out state is achieved through the exchange interaction; this allows us to keep the dipolar interaction small. Field misalignment can also be minimized by using a vector magnet [33]. The observation of charge order at temperatures much higher than that characterizing both the residual field and dipolar energy scales would be a strong indication of OBD. Detecting the AFM order disappear as a function of increasing field [see Fig. 1(c)] would also be a conclusive smoking gun. Neutron scattering could be a sensitive probe if only short- or medium-range AFM order is set due to competing ordering trends. A second route towards OBD is to take advantage of

the recent advances in the design of frustrated magnets to create a planar system similar to the one in Fig. 1(b), thus minimizing problems of field misalignment. The idea is to use artificial square-lattice spin-ice samples in their AFM phase, with the vertex energy hierarchy $\epsilon_c < \epsilon_e < \epsilon_{a,b}$, where c indicates AFM, e represents three-in–one-out or three-out–one-in, and a, b represent FM vertices [11,34] (see the Supplemental Material for a detailed explanation [26]). The third route concerns the use of colloidal systems in 2D arrays of optical traps, where staggered charge order could be attainable [12,35]. The precise control over the interactions and accessibility of thermal excitations may offer another fertile ground to recreate this experiment. As we have seen, FSE have a very strong influence in ρ_S^s; this fact may be exploited to recognize incipient OBD using samples with small size.

In summary, we have made an in-depth numerical and theoretical study of OBD in two models closely linked to ice systems. Our results may establish a route to the much-sought-after experimental realization of classical order by disorder.

We thank P. Holdsworth, L. Jaubert, C. Marrows, and R. Moessner for very useful discussions. This work was supported in part by MINCyT-ECOS A14E01, PICS 506691 (CNRS-CONICET), NSF under Grant No. PHY11-25915, ANPCyT through PICT 2013 No. 2004 and PICT 2014 No. 2618, and Consejo Nacional de Investigaciones Científicas y Técnicas (CONICET). M. V. F. acknowledges partial financial support from Universidad Nacional de La Pampa, Argentina. L. F. C. is a member of the Institut Universitaire de France.

*r.chufo@gmail.com

[1] J. Villain, R. Bidaux, J.-P. Carton, and R. Conte, J. Phys. **41**, 1263 (1980).
[2] J. T. Chalker, in *Introduction to Frustrated Magnetism: Materials, Experiments, Theory*, edited by C. Lacroix, P. Mendels, and F. Mila (Springer Science & Business Media, Berlin, 2011), pp. 3–22.
[3] M. K. Phani, J. L. Lebowitz, and M. H. Kalos, Phys. Rev. B **21**, 4027 (1980).
[4] J. D. M. Champion, M. J. Harris, P. C. W. Holdsworth, A. S. Wills, G. Balakrishnan, S. T. Bramwell, E. Čižmár, T. Fennell, J. S. Gardner, J. Lago, D. F. McMorrow, M. Orendáč, A. Orendáčová, D. M. Paul, R. I. Smith, M. T. F. Telling, and A. Wildes, Phys. Rev. B **68**, 020401 (2003).
[5] M. E. Zhitomirsky, M. V. Gvozdikova, P. C. W. Holdsworth, and R. Moessner, Phys. Rev. Lett. **109**, 077204 (2012).
[6] L. Savary, K. A. Ross, B. D. Gaulin, J. P. C. Ruff, and L. Balents, Phys. Rev. Lett. **109**, 167201 (2012).
[7] K. A. Ross, Y. Qiu, J. R. D. Copley, H. A. Dabkowska, and B. D. Gaulin, Phys. Rev. Lett. **112**, 057201 (2014).
[8] J. N. Reimers, J. E. Greedan, C. V. Stager, M. Bjorgvinnsen, and M. A. Subramanian, Phys. Rev. B **43**, 5692 (1991).
[9] A. Sadeghi, M. Alaei, F. Shahbazi, and M. J. P. Gingras, Phys. Rev. B **91**, 140407(R) (2015).
[10] V. K. Anand, A. K. Bera, J. Xu, T. Herrmannsdörfer, C. Ritter, and B. Lake, Phys. Rev. B **92**, 184418 (2015).
[11] C. H. Marrows (private communication).
[12] C. J. Olson Reichhardt, A. Libál, and C. Reichhardt, New J. Phys. **14**, 025006 (2012).
[13] R. G. Melko and M. J. P. Gingras, J. Phys. Condens. Matter **16**, R1277 (2004).
[14] R. A. Borzi, D. Slobinsky, and S. A. Grigera, Phys. Rev. Lett. **111**, 147204 (2013).
[15] M. E. Brooks-Bartlett, S. T. Banks, L. D. C. Jaubert, A. Harman-Clarke, and P. C. W. Holdsworth, Phys. Rev. X **4**, 011007 (2014).
[16] Y.-L. Xie, Z.-Z. Du, Z.-B. Yan, and J.-M. Liu, Sci. Rep. **5**, 15875 (2015).
[17] L. Foini, D. Levis, M. Tarzia, and L. F. Cugliandolo, J. Stat. Mech. (2013) P02026.
[18] J. Lukic, E. Marinari, and O. C. Martin, Europhys. Lett. **73**, 779 (2006).
[19] Z. Hiroi, K. Matsuhira, and M. Ogata, J. Phys. Soc. Jpn. **72**, 3045 (2003).
[20] S. T. Bramwell and M. J. P. Gingras, Science **294**, 1495 (2001).
[21] C. Castelnovo, R. Moessner, and S. L. Sondhi, Nature (London) **451**, 42 (2008).
[22] P. C. Guruciaga, S. A. Grigera, and R. A. Borzi, Phys. Rev. B **90**, 184423 (2014).
[23] $\mathbf{B}\|[100]$ also has this property, but it does not lead to a single-charge ground state.
[24] T. Sakakibara, T. Tayama, Z. Hiroi, K. Matsuhira, and S. Takagi, Phys. Rev. Lett. **90**, 207205 (2003).
[25] F. Wang and D. P. Landau, Phys. Rev. Lett. **86**, 2050 (2001).
[26] See Supplemental Material at http://link.aps.org/supplemental/10.1103/PhysRevLett.117.167203, which includes Ref. [27], for simulation methods and further analysis of numerical data, as well as details on the antiferromagnetic ground state for artificial spin ice.
[27] R. E. Belardinelli and V. D. Pereyra, Phys. Rev. E **75**, 046701 (2007).
[28] D. Levis, L. F. Cugliandolo, L. Foini, and M. Tarzia, Phys. Rev. Lett. **110**, 207206 (2013).
[29] L. F. Cugliandolo, G. Gonnella, and A. Pelizzola, J. Stat. Mech. (2015) P06008.
[30] Note that the number of spins on two neighboring columns in the direction y' may differ by 2. However, for M large enough, this gives subleading boundary corrections which we will neglect in the following.
[31] R. Moessner, Can. J. Phys. **79**, 1283 (2001).
[32] J. Xu, V. K. Anand, A. K. Bera, M. Frontzek, D. L. Abernathy, N. Casati, K. Siemensmeyer, and B. Lake, Phys. Rev. B **92**, 224430 (2015).
[33] J. A. N. Bruin, R. A. Borzi, S. A. Grigera, A. W. Rost, R. S. Perry, and A. P. Mackenzie, Phys. Rev. B **87**, 161106 (2013).
[34] J. P. Morgan, A. Stein, S. Langridge, and C. H. Marrows, Nat. Phys. **7**, 75 (2011).
[35] A. Ortíz-Ambriz and P. Tierno, Nat. Commun. **7**, 10575 (2016).